The Three-Dimensional Algorithm of Solving the Electric Field Integral Equation Using Face-Centered Node Points, Conjugate Gradient Method, and FFT

Ching-Chuan Su

Abstract—**It has been known for a long time that the accuracy of solving the scattering by a dielectric body using the electric field integral equation (EFIE) is poor when the permittivity of the scatterer becomes large. Recently, such a trouble has been settled by using a procedure involving face-centered node points. Such a procedure is efficient, since it preserves the convolution property in the EFIE and, hence, the applicability of the fast Fourier transform. In this investigation we generalize this procedure to the three-dimensional and anisotropic case. The generalization is quite straight in both the formulation and the programming. A calculation for a scatterer with a relative permittivity as high as 100 indicates that the proposed procedure converges quite rapidly, while the conventional approach fails to converge in using the conjugate gradient method.**

I. Introduction

TO CALCULATE the scattering by a homogeneous dielectric body with arbitrary shape, methods involving surface integral equations have been developed [1]–[3], where the unknown fields appear only on the scatterer surface. For an inhomogeneous body the scattering problem is much more involved, since the unknown fields to be solved are distributed within the entire body. In the special case of a "body of revolution," the scattering problem can be reduced to a two-dimensional one, for which a method employing the finite-element technique has been proposed [4]. For a general three-dimensional scatterer, methods for solving time-harmonic Maxwell's equations in the differential form (using the finite-element or finite-difference technique) may be too complicated and do not yet appear in the literature, to our knowledge. To deal with such a general problem, the method based on the electric field integral equation is widely employed. To solve the integral equation numerically, the method employing the block model in conjunction with the pulse-function expansion and the point-matching technique is simple in the programming and is quite popular [5]–[7]. Moreover, the efficiency of this method in both the computational speed and memory requirement can be greatly improved by a use of the conjugate gradient method (CGM) and the fast Fourier transform (FFT) [8]–[10].

Recently, it has been pointed out that condition numbers of the resulting matrices increase as the permittivities are increased, if the conventional numerical procedure is used [9]. Since the solutions are sensitive to minor variations in the elements of ill-conditioned matrices, one has to model the scatterer accurately by using more flexible cells and employ higher-order basis functions [11]–[13]. Essentially, such procedures do not improve the conditions of the resulting matrices. Furthermore, since the convolution property in the EFIE may be deteriorated, the memory requirement is prohibitively large and the efficient FFT can not be applied.

To attack such a trouble, we have proposed a new procedure using the face-centered node points [14]. Such a procedure is more accurate, since the condition numbers of the corresponding matrices can be kept small, regardless of the magnitudes of the permittivity. And the polarization charge induced at the cell surfaces can be modeled more accurately. Furthermore, this procedure is efficient, since the convolution property in the EFIE is preserved. In this investigation, we generalize this algorithm involving face-centered node points, the CGM, and the FFT to deal with the electromagnetic scattering from a three-dimensional and anisotropic (biaxial) dielectric body.

II. Electric Field Integral Equation

The electric field $\boldsymbol{E}$ due to time-harmonic current and charge sources radiating in free space with angular frequency ω can be written in terms of the magnetic vector potential $\boldsymbol{A}$ and the electric scalar potential $\boldsymbol{\Phi}$:

$$\boldsymbol{E}(\boldsymbol{r}) = \boldsymbol{E}^i(\boldsymbol{r}) - j\omega\boldsymbol{A}(\boldsymbol{r}) - \nabla\boldsymbol{\Phi}(\boldsymbol{r}). \tag{1}$$

Here

$$\boldsymbol{A}(\boldsymbol{r}) = \mu_0 \int\int\int G(k_0R)\boldsymbol{J}(\boldsymbol{r}')\,d\boldsymbol{r}' \tag{2a}$$

$$\boldsymbol{\Phi}(\boldsymbol{r}) = \frac{1}{\epsilon_0}\int\int\int G(k_0R)\rho(\boldsymbol{r}')\,d\boldsymbol{r}', \tag{2b}$$

$G(k_0R) = \exp(-jk_0R)/4\pi R$ denotes Green's function in free space, $R = |\boldsymbol{r}-\boldsymbol{r}'|$, $k_0 = \omega\sqrt{\mu_0\epsilon_0}$, and $\boldsymbol{J}$ and ρ denote, respectively, the electric current and charge density distributions, excluding the sources generating the incident electric field $\boldsymbol{E}^i$. Consider the scattering problem of a dielectric body composed of biaxial material, of which the off-diagonal components of the tensor permittivity distribution $\epsilon_0\bar{\bar{\epsilon}}(r)$ are zero. Expressing

Manuscript received October 24, 1991; revised July 21, 1992.

The author is with the Department of Electrical Engineering, National Tsinghua University, Hsinchu, Taiwan, 30043, Republic of China.

IEEE Log Number 9205454.

the polarization current density $\boldsymbol{J}$ and polarization charge density ρ in terms of $\boldsymbol{E}$, one obtains the electric field integral equation

$$\boldsymbol{E}(\boldsymbol{r}) = \boldsymbol{E}^i(\boldsymbol{r}) + k_0^2 \int\int\int G(k_0R)\bar{\bar{\chi}}(\boldsymbol{r}') \cdot \boldsymbol{E}(\boldsymbol{r}')\, d\boldsymbol{r}' - \frac{1}{\epsilon_0}\nabla \int\int\int G(k_0R)\rho(\boldsymbol{r}')\, d\boldsymbol{r}', \tag{3}$$

where $\bar{\bar{\chi}} = \bar{\bar{\epsilon}} - \bar{\bar{I}}$, and $\bar{\bar{I}}$ is the unit dyad. Using the continuity equation the polarization charge density ρ in (3) can be expressed as

$$\rho(\boldsymbol{r}) = -\epsilon_0 \nabla \cdot [\bar{\bar{\chi}}(\boldsymbol{r}) \cdot \boldsymbol{E}(\boldsymbol{r})] \tag{4a}$$

$$= \epsilon_0 \nabla \cdot \boldsymbol{E}(\boldsymbol{r}). \tag{4b}$$

In obtaining (4b) the continuity of displacement $\nabla \cdot (\bar{\bar{\epsilon}} \cdot \boldsymbol{E}) = 0$ has been made use of and hence (4b) is valid only for those regions having no free charge sources. The integrations in (3) are over the interior and the surface of the scatterer. Thus, the surface charges, which may reside on the scatterer surface, have been taken into account. Equation (3) consists of three coupled integral equations in terms of E_x, E_y, and E_z, and the resultant field $\boldsymbol{E}(\boldsymbol{r})$ should be found by solving the three coupled integral equations implied in (3).

III. Numerical Procedure for Face-Centered Node Points

Scattering from an arbitrary body is identical to that from a rectangular body composed of the arbitrarily-shaped scatterer and the surrounding space with $\bar{\bar{\chi}} = 0$. Divide the rectangular body into $m_1 \times m_2 \times m_3$ identical cells which are rectangular parallelepipeds of volume $\Delta v = \Delta x \times \Delta y \times \Delta z$ (Fig. 1). Since the node points are located at the cell surfaces, the $(m_1 - 1) \times (m_2 - 1) \times (m_3 - 1)$ cells should enclose the entire scatterer. Suppose the cells are small enough that the three components in $\bar{\bar{\epsilon}}(x, y, z)$ may be treated as constant over each of the cells. Thereafter, pulse-function expansion and point-matching technique are employed in the numerical calculation. As in [14], in order to keep the resulting matrix well-conditioned and to represent the induced polarization charge more accurately, the node points at which the fields are to be solved are not placed at the center of each cell; rather, are placed at the centers of the faces of each rectangular parallelepiped. And, the x, y, and z components of the electric field are sampled and matched at the face-centered node points marked crosses, squares, and dots, respectively (Fig. 1), such that all these fields are the normal components with respect to the corresponding faces.

No polarization charges are induced in a homogeneous medium, isotropic or anisotropic. Thus, in the block model, the polarization charges are induced only on the faces of cells and can be determined from the normal components of the electric fields at the faces. From the continuity of displacement it is known that the x component of the field and the permittivity distribution satisfy the following relation at the face separating

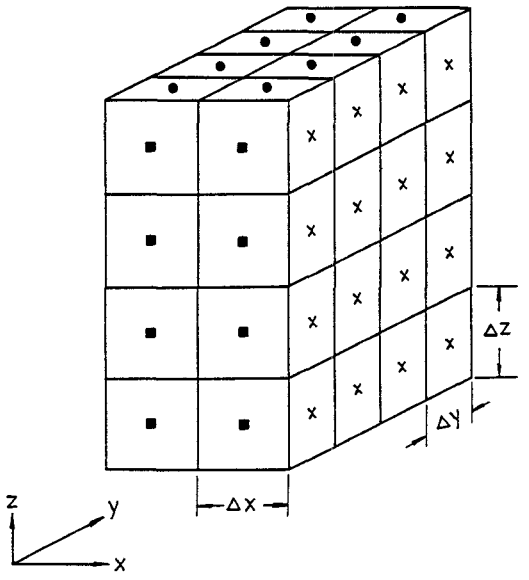

Fig. 1. An rectangular body composed of $m_1 \times m_2 \times m_3$ identical, rectangular cells with volume $\Delta v = \Delta x \times \Delta y \times \Delta z$. The $(m_1 - 1) \times (m_2 - 1) \times (m_3 - 1)$ cells should enclose the entire scatterer. The crosses ($\times$), squares (■), and dots (•) are the face-centered node points, at which the E_x, E_y, and E_z are to be sampled and matched, respectively.

cells (i, j, k) and $(i - 1, j, k)$:

$$\epsilon_x(i, j, k)E_{x1} = \epsilon_x(i - 1, j, k)E_{x2}, \tag{5}$$

where E_{x1} and E_{x2} are the fields at the center of this face, approaching from cells (i, j, k) and $(i - 1, j, k)$, respectively. At a face separating two blocks of dissimilar media the charge density becomes impulsive. From (4b) and (5) the corresponding surface charge density ρ_{sx} at this face-centered node points can be given by either one of the following two formulas in terms of E_{x2} or E_{x1}:

$$\rho_{sx} = \epsilon_0 E_{x2}[\epsilon_x(i - 1, j, k) - \epsilon_x(i, j, k)]/\epsilon_x(i, j, k) \tag{6a}$$

$$= \epsilon_0 E_{x1}[\epsilon_x(i - 1, j, k) - \epsilon_x(i, j, k)]/\epsilon_x(i - 1, j, k). \tag{6b}$$

A key step of the proposed method is: we choose either (6a) or (6b) as the formula to represent the surface charge density in the integral equation (3) and, hence, take either E_{x2} or E_{x1} as an unknown field (designated $E_x(i, j, k)$ hereafter) to be solved according to whether $\epsilon_x(i, j, k)$ or $\epsilon_x(i - 1, j, k)$ is larger in magnitude. By this algorithm, the large one between $\epsilon_x(i, j, k)$ and $\epsilon_x(i - 1, j, k)$ always appears on the denominator in the chosen formula. Consequently, the off-diagonal elements in the resulting matrix and hence the condition number can be kept small, regardless of the magnitudes of the permittivities involved. In this manner, the node point is not exactly placed at the face, but approaches the face from the side where the permittivity is smaller. The same procedure is used to choose the y and z components as unknown fields in the integral equation.

Then, on applying the pulse functions to expand the unknown field $\boldsymbol{E}(\boldsymbol{r})$ and using the point-matching technique, the integral equation (3) reduces to a set of $3M$ ($M = m_1 \times m_2 \times m_3$) simultaneous linear equations in terms of

$3M$ unknowns $\boldsymbol{E}(i,j,k)$ as

$$\begin{aligned} E_\mu(i,j,k) = {} & E^i_\mu(i,j,k) + s_\mu(i,j,k)\hat{\chi}_\mu(i,j,k)E_\mu(i,j,k) \\ & + \sum_{i'=0}^{m_1-1}\sum_{j'=0}^{m_2-1}\sum_{k'=0}^{m_3-1}\Bigg\{ g(i-i',j-j',k-k') \\ & \cdot \chi_\mu(i',j',k')E_\mu(i',j',k') \\ & + \sum_{\nu=x,y,z} g_{\mu\nu}(i-i',j-j',k-k') \\ & \cdot\hat{\chi}_\nu(i',j',k')E_\nu(i',j',k')\Bigg\}, \\ & \mu = x,y,z \\ & i = 0,1,\cdots m_1-1 \\ & j = 0,1,\cdots m_2-1 \\ & k = 0,1,\cdots m_3-1 \end{aligned} \tag{7}$$

where $E^i_\mu(i,j,k)$ denotes the incident field at an associated face-centered node point at which the field $E_\mu(i,j,k)$ is sampled. The function g denotes the value of k_0^2 times the integral of Green's function over a cell and its numerical values can be approximated as

$$g(i,j,k) = \begin{cases} -1 + e^{-jk_0a}(1+jk_0a) \\ \quad i=0, j=0, \text{ and } k=0 \\ k_0^2 G(k_0R)\Delta v, \\ \quad \text{otherwise} \end{cases} \tag{8}$$

where $a^3 = 3\Delta v/4\pi$ and $R^2 = (i\Delta x)^2 + (j\Delta y)^2 + (k\Delta z)^2$. (Do not confuse the purely imaginary number j with index j.) The functions g_{xx}, g_{yx}, and g_{zx} are given as the integrals of the x, y, and z components of ∇G over a face of size $\Delta y \times \Delta z$, respectively. They can be evaluated numerically in a way similar to that in [10]. For larger arguments, simple formulas without numerical itegration can be given as

$$g_{xx}(i,j,k) = -\Delta y\Delta z(1+jk_0R)e^{-jk_0R}(i\Delta x)/4\pi R^3, \quad i\neq 0, j\neq 0, \text{ or } k\neq 0 \tag{9a}$$

$$g_{yx}(i,j,k) = \Delta z[G(k_0R_1) - G(k_0R_2)], \tag{9b}$$

and

$$g_{zx}(i,j,k) = \Delta y[G(k_0R_1) - G(k_0R_3)], \tag{9c}$$

where

$$R_1 = \{[(i+0.5)\Delta x]^2 + [j\Delta y]^2 + [k\Delta z]^2\}^{1/2},$$
$$R_2 = \{[(i+0.5)\Delta x]^2 + [(j-1)\Delta y]^2 + [k\Delta z]^2\}^{1/2},$$

and

$$R_3 = \{[(i+0.5)\Delta x]^2 + [j\Delta y]^2 + [(k-1)\Delta z]^2\}^{1/2}.$$

The other $g_{\mu\nu}$ functions can be obtained in a similar way. For $g_{\mu\mu}(0,0,0)$ an analytical integration yields $\pm\frac{1}{2}$, depending on the associated face-centered node point approaches the face from which side. Such indefinite terms deteriorate the convolution property in the EFIE. To avoid this trouble, we let $g_{xx}(0,0,0) = g_{yy}(0,0,0) = g_{zz}(0,0,0) = 0$ and, accordingly, introduce

$$s_x(i,j,k) = \begin{cases} \frac{1}{2} & |\epsilon_x(i,j,k)| > |\epsilon_x(i-1,j,k)| \\ -\frac{1}{2}, & \text{otherwise} \end{cases} \tag{10a}$$

$$s_y(i,j,k) = \begin{cases} \frac{1}{2} & |\epsilon_y(i,j,k)| > |\epsilon_y(i,j-1,k)| \\ -\frac{1}{2}, & \text{otherwise} \end{cases} \tag{10b}$$

and

$$s_z(i,j,k) = \begin{cases} \frac{1}{2} & |\epsilon_z(i,j,k)| > |\epsilon_z(i,j,k-1)| \\ -\frac{1}{2}, & \text{otherwise} \end{cases} \tag{10c}$$

The functions $\hat{\chi}_\mu$ and χ_μ in (7) correspond to the effects of the induced polarization charge and current, respectively. They are given by

$$\hat{\chi}_x(i,j,k) = \{\epsilon_x(i,j,k) - \epsilon_x(i-1,j,k\}/\epsilon_{x\max}, \tag{11a}$$
$$\hat{\chi}_y(i,j,k) = \{\epsilon_y(i,j,k) - \epsilon_y(i,j-1,k\}/\epsilon_{y\max}, \tag{11b}$$
$$\hat{\chi}_z(i,j,k) = \{\epsilon_z(i,j,k) - \epsilon_z(i,j,k-1\}/\epsilon_{z\max}, \tag{11c}$$

$$\chi_x(i,j,k) = \{\epsilon_x(i,j,k)\epsilon_x(i-1,j,k) - \tfrac{1}{2}[\epsilon_x(i,j,k) + \epsilon_x(i-1,j,k)]\}/\epsilon_{x\max}, \tag{12a}$$

$$\chi_y(i,j,k) = \{\epsilon_y(i,j,k)\epsilon_y(i,j-1,k) - \tfrac{1}{2}[\epsilon_y(i,j,k) + \epsilon_y(i,j-1,k)]\}/\epsilon_{y\max}, \tag{12b}$$

and

$$\chi_z(i,j,k) = \{\epsilon_z(i,j,k)\epsilon_z(i,j,k-1) - \tfrac{1}{2}[\epsilon_z(i,j,k) + \epsilon_z(i,j,k-1)]\}/\epsilon_{z\max}, \tag{12c}$$

where $\epsilon_{x\max}, \epsilon_{y\max}$, and $\epsilon_{z\max}$ denote the larger ones in magnitude between $\epsilon_x(i,j,k)$ and $\epsilon_x(i-1,j,k)$, $\epsilon_y(i,j,k)$ and $\epsilon_y(i,j-1,k)$, and between $\epsilon_z(i,j,k)$ and $\epsilon_z(i,j,k-1)$, respectively. In writing (12), the contribution of the polarization current is averaged between two adjacent cells. Note that at an interface separating two blocks of similar media, the polarization charge is set to zero automatically, as it should be.

As discussed in the two-dimensional counterpart [14], with the $\epsilon_{x\max}, \epsilon_{y\max}$, and $\epsilon_{z\max}$ emerging on the denominators in (11), the condition number of the resulting matrix is kept small, regardless of the magnitude of the permittivity distribution. Consequently, the simple block model in conjunction with the pulse-function expansion and point-matching technique works well. Thereby, the convolution property in the EFIE and hence the applicability of the FFT can be preserved.

IV. Solution Procedure Using CGM and FFT

Simultaneous equations (7) can be arranged in a $3M \times 3M$ matrix equation

$$\boldsymbol{Ax} = \boldsymbol{b}, \tag{13}$$

where, $\boldsymbol{A}$ is a $3M \times 3M$ full matrix whose entries correspond to $g, g_{\mu\nu}, \chi_\mu$, and $\hat{\chi}_\mu$, and x and $\boldsymbol{b}$ are $3M$-dimensional vectors whose components correspond to $E_\mu(i,j,k)$ and $E^i_\mu(i,j,k)$, respectively. One can obtain the solution $\boldsymbol{x}$ by inverting the matrix $\boldsymbol{A}$. Such an inverting procedure is inefficient, however; since it requires $(3M)^2$ storage locations of complex data and

a computation time of $(3M)^3/3$ times T_c, where T_c denotes the computation time for a complex multiplication. In this investigation we employ the conjugate gradient method and the FFT to solve (7) or, equivalently, the matrix equation (13). Such a procedure is more efficient, in that it requires only about 160M storage locations of complex data and a computation time about $30M^2 \log_2 M$ times T_c.

The conjugate gradient method (CGM) [15], [16] begins with an arbitrary starting vector $\boldsymbol{x}_0$, from which one evaluates the residue vector $\boldsymbol{r}_0$ by the formula

$$\boldsymbol{r}_0 = \boldsymbol{b} - \boldsymbol{A}\boldsymbol{x}_0. \tag{14}$$

Then, each iteration step consists of the operations evaluating the orthogonalization coefficient ξ_ℓ, the correction direction vector d_ℓ, the correction coefficient γ_ℓ, the new solution $\boldsymbol{x}_{\ell+1}$, and the new residue $\boldsymbol{r}_{\ell+1}$ by the following formulas

$$\xi_\ell = \begin{cases} 0 & \ell = 0 \\ ||\tilde{\boldsymbol{A}}\boldsymbol{r}_\ell||^2/||\tilde{\boldsymbol{A}}\boldsymbol{r}_{\ell-1}||^2, & \ell = 1,2\cdots \end{cases} \tag{15a}$$

$$\boldsymbol{d}_\ell = \tilde{\boldsymbol{A}}\boldsymbol{r}_\ell + \xi_\ell \boldsymbol{d}_{\ell-1}, \qquad \ell = 0,1,2\cdots \tag{15b}$$

$$\gamma_\ell = ||\tilde{\boldsymbol{A}}\boldsymbol{r}_\ell||^2/||\boldsymbol{A}\boldsymbol{d}_\ell||^2, \tag{15c}$$

$$\boldsymbol{x}_{\ell+1} = \boldsymbol{x}_\ell + \gamma_\ell \boldsymbol{d}_\ell, \tag{15d}$$

and

$$\boldsymbol{r}_{\ell+1} = \boldsymbol{r}_\ell - \gamma_\ell \boldsymbol{A}\boldsymbol{d}_\ell, \tag{15e}$$

where $\tilde{\boldsymbol{A}} = (\boldsymbol{A}^*)^t$, superscripts * and t mean complex conjugate and transpose, respectively. In (15), the square of the norm of a vector $\boldsymbol{v}$, $||\boldsymbol{v}||^2$, is defined as $(\boldsymbol{v}*)^t\boldsymbol{v}$. The key point of this method is that using the formulas given in (15), the calculated vectors $\tilde{\boldsymbol{A}}\boldsymbol{r}_\ell$, $\ell = 0,1\cdots$, become mutually orthogonal. Then, for a nonsingular matrix $\boldsymbol{A}$ of order n, $\tilde{\boldsymbol{A}}\boldsymbol{r}_\ell$ and hence $\boldsymbol{r}_\ell$ will become null vectors for $\ell \geq n$. That is one will obtain a numerically exact solution with at most n iteration steps, if the round-off error can be neglected. In this investigation the termination criterion is defined as $||\boldsymbol{r}_\ell||/||\boldsymbol{b}|| < 10^{-4}$.

It is obvious that the major computation in each iteration step lies in the two multiplications: $\boldsymbol{A}\boldsymbol{d}_\ell$ and $\tilde{\boldsymbol{A}}\boldsymbol{r}_\ell$ or, equivalently, the $6M$ summations shown in (16a) and (16b) at the bottom of the page, with $\mu = x,y,z, i = 0,1,\cdots m_1-1, j = 0,1,\cdots m_2-1$, and $k = 0,1,\cdots m_3-1$. In (16), the three-dimensional $m_1 \times m_2 \times m_3$ arrays $D_\mu(i,j,k)$ and $R_\mu(i,j,k)$ correspond to vectors $\boldsymbol{d}_\ell$ and $\boldsymbol{r}_\ell$, respectively. It needs about $24M^2$ multiplications for the $6M$ summations. However, it is seen that the triple summations involved in (16) is of the form of three-dimensional convolution and hence can be performed using the three-dimensional fast Fourier transform (FFT) as

$$D_\mu(i,j,k) - s_\mu(i,j,k)\hat{\chi}_\mu(i,j,k)D_\mu(i,j,k) - F_{ijk}^{-1}\left\{F[g]F[\chi_\mu D_\mu] + \sum_{\nu=x,y,z} F[g_{\mu\nu}]F[\hat{\chi}_\nu D_\nu]\right\} \tag{17a}$$

and

$$R_\mu(i,j,k) - s_\mu(i,j,k)\hat{\chi}_\mu^*(i,j,k)R_\mu(i,j,k) - \chi_\mu^*(i,j,k)F_{ijk}^{-1}\{F[g]^*F[R_\mu]\} - \hat{\chi}_\mu^*(i,j,k)F_{ijk}^{-1}\left\{\sum_{\nu=x,y,z} F[g_{\nu\mu}]^*F[R_\nu]\right\}, \tag{17b}$$

where F_{ijk}^{-1} denotes entry ijk in the resulting three-dimensional array after the inverse FFT, and F means an FFT operating on an $n_1 \times n_2 \times n_3$ three-dimensional array with $n_1 \geq 2m_1 - 1, n_2 \geq 2m_2 - 1, n_3 \geq 2m_3 - 1$, and n_1, n_2, and n_3 are chosen to be integer powers of 2. The arguments of the functions $g(i,j,k)$ and $g_{\mu\nu}(i,j,k)$ are within $-m_1 < i < m_1, -m_2 < j < m_2$, and $-m_3 < k < m_3$. In (17), we make g and $g_{\mu\nu}$ be $n_1 \times n_2 \times n_3$ (periodic) arrays, by letting the functional values be zero when the arguments lie outside the ranges. Accordingly, we have extended the $m_1 \times m_2 \times m_3$ arrays D_μ and R_μ into $n_1 \times n_2 \times n_3$ arrays, with $D_\mu(i,j,k) = R_\mu(i,j,k) = 0$, when $m_1 \leq i \leq n_1 - 1, m_2 \leq j \leq n_2 - 1$, or $m_3 \leq k \leq n_3 - 1$. In (17b) we also made use of the property

$$D_\mu(i,j,k) - s_\mu(i,j,k)\hat{\chi}_\mu(i,j,k)D_\mu(i,j,k) - \sum_{i'=0}^{m_1-1}\sum_{j'=0}^{m_2-1}\sum_{k'=0}^{m_3-1}\left\{g(i-i',j-j',k-k')\chi_\mu(i',j',k')D_\mu(i',j',k') - \sum_{\nu=x,y,z} g_{\mu\nu}(i-i',j-j',k-k')\hat{\chi}_\nu(i',j',k')D_\nu(i',j',k')\right\}, \tag{16a}$$

and

$$R_\mu(i,j,k) - s_\mu(i,j,k)\hat{\chi}_\mu^*(i,j,k)R_\mu(i,j,k) - \chi_\mu^*(i,j,k)\sum_{i'=0}^{m_1-1}\sum_{j'=0}^{m_2-1}\sum_{k'=0}^{m_3-1} g^*(i'-i,j'-j,k'-k)R_\mu(i',j',k') - \hat{\chi}_\mu^*(i,j,k)\sum_{\nu=x,y,z}\sum_{i'=0}^{m_1-1}\sum_{j'=0}^{m_2-1}\sum_{k'=0}^{m_3-1} g_{\nu\mu}^*(i'-i,j'-j,k'-k)R_\nu(i',j',k'), \tag{16b}$$

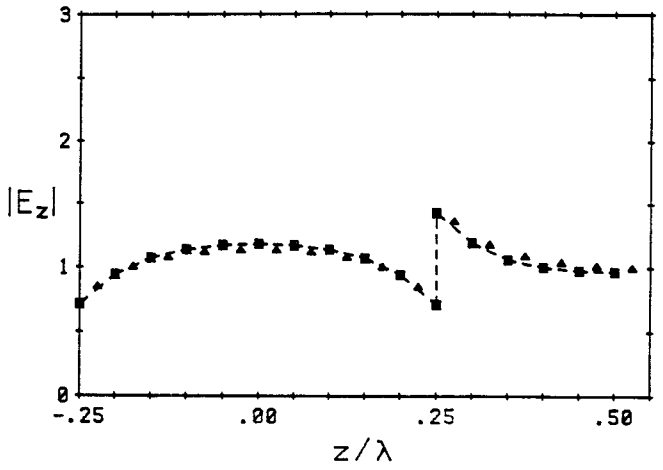

Fig. 2. Field distribution along the z direction at $x = y = 0$. The relative permittivity $\epsilon = 2, L = 0.5\lambda$, and $A_c = (0.15\lambda)^2$. The squares (■) and triangles (▲) are the results calculated using the present method and that in [10], respectively. The z component of the electric field is discontinuous at $z = \pm 0.25\lambda$, the ends of this finite cylinder.

$F[f^*(-i,-j,-k)] = F[f(i,j,k)]^*$, where f is an arbitrary $n_1 \times n_2 \times n_3$ periodic array [17]. The FFT's pertaining to g and $g_{\mu\nu}$ are performed once for all iteration steps. These transforms needs $10N$ storage locations of complex data, where $N = n_1 \times n_2 \times n_3$. The major computation in each iteration step requires 18 $n_1 \times n_2 \times n_3$-point FFT's, each FFT in turn requires about $N(log_2 N)$ complex multiplications.

V. Numerical Results

To check the accuracy of the proposed method, we compare the results calculated using the present and the conventional procedures [10]. We consider a homogeneous, isotropic cylinder with a finite length L in the z direction and a square cross section of size A_c. This finite cylinder has a small relative permittivity $\epsilon = 2, L = 0.5\lambda$, and $A_c = (0.15\lambda)^2$, where λ is the wavelength in free space. The incident field is assumed to be a plane wave, $\boldsymbol{E}^i = \hat{z}e^{-jk_0x}$. The associated field distributions along z at $x = 0, y = 0$ (the origin of the coordinates is located at the center of the scatterer) are shown in Fig. 2. It is seen that these two results are in good agreement. When the permittivity ϵ is increased to as large as 100, the CGM iteration process in the conventional procedure [10] does not converge at all. Whereas, the present procedure converges quite rapidly. The field distributions are shown in Fig. 3. The scatterer is modeled with $3 \times 3 \times 10$ cubic cells (while, $m_1 = 4, m_2 = 4$, and $m_3 = 16$). For the cases in Fig. 3(a) and (b), the cell size is 0.1 and 0.05 internal wavelength and the number of iteration to reach convergence is 27 and 35 (the number of unknowns is 768), respectively.

VI. Conclusion

The procedure involving face-centered node points has been generalized to the three-dimensional and anisotropic (biaxial) case. Thus, the scattering from a dielectric body with a large permittivity can be handled. Since the resulting matrices are well-conditioned, the simple pulse-basis block model can be used. An important benefit is that the convolution

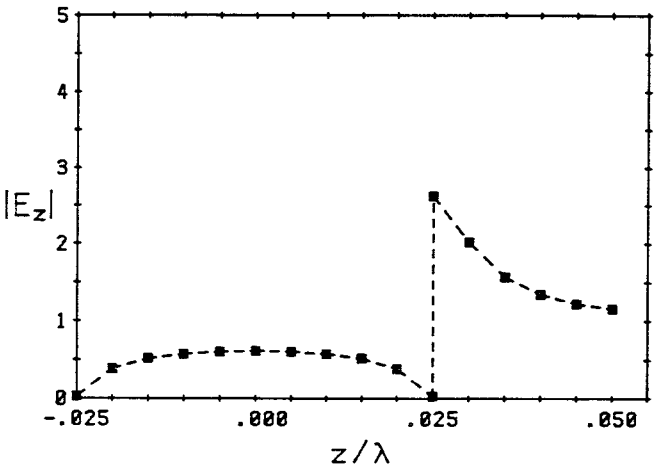

(a)

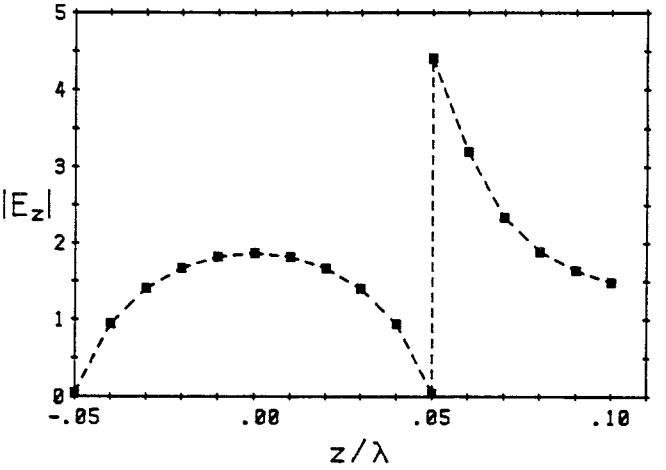

(b)

Fig. 3. Field distributions along the z direction at $x = y = 0$. The relative permittivity $\epsilon = 100$. (a) $L = 0.05\lambda, A_c = (0.015\lambda)^2$; (b) $L = 0.1\lambda, A_c = (0.03\lambda)^2$.

property in the EFIE is preserved and, hence, the FFT can be applied. This efficient solution procedure requires about 160M complex storage locations and a total computational task of about $30M^2 \log_2 M$ complex multiplications. The saving in computational cost becomes more significant for larger scatterers and/or finer discretizations, where the number of cells M is increased.

The calculations made in this investigation were performed on a personal computer where the maximum M was limited to 256. Ten times this number or more may be possible on a larger machine. Since the major computational task lies in the calculation of FFT, the speed of the proposed method may be greatly improved if a hardware FFT processor is used.

References

[1] P. Barber and C. Yeh, "Scattering of electromagnetic waves by arbitrarily shaped dielectric bodies," *Appl Opt.*, vol. 14, pp. 2864–2872, Dec. 1975.

[2] T. K. Wu and L. L. Tsai, "Scattering from arbitrarily-shaped lossy dielectric bodies of revolution," *Radio Sci.*, vol. 12, pp. 709–718, Sept. 1977.

[3] K. Umashankar, A. Taflove, and S. M. Rao, "Electromagnetic scattering by arbitrary shaped three-dimensional homogeneous lossy dielectric

objects," *IEEE Trans. Antennas Propagat.*, vol. AP-34, pp. 758–765, June 1986.
[4] M. A. Morgan and K. K. Mei, "Finite-element computation of scattering by inhomogeneous penetrable bodies of revolution," *IEEE Trans. Antennas Propagat.*, vol. AP-27, pp. 202–214, Mar. 1979.
[5] D. E. Livesay and K. M. Chen, "Electromagnetic fields induced inside arbitrarily shaped biological bodies," *IEEE Trans. Microwave Theory Tech.*, vol. MTT-22, pp. 1273–1280, Dec. 1974.
[6] K. M. Chen and B. S. Guru, "Internal EM field and absorbed power density in human torsos induced by 1–500-MHz EM waves," *IEEE Trans. Microwave Theory Tech.*, vol. MTT-25, pp. 746–756, Sept. 1977.
[7] M. J. Hagmann, O. P. Gandhi, and C. H. Durney, "Numerical calculation of electromagnetic energy deposition for a realistic model of man," *IEEE Trans. Microwave Theory Tech.*, vol. MTT-27, pp. 804–809, Sept. 1979.
[8] D. T. Borup and O. P. Gandhi, "Calculation of high-resolution SAR distributions in biological bodies using the FFT algorithm and conjugate gradient method," *IEEE Trans. Microwave Theory Tech.*, vol. MTT-33, pp. 417–419, May 1985.
[9] C. C. Su, "Calculation of electromagnetic scattering from a dielectric cylinder using the conjugate gradient method and FFT," *IEEE Trans. Antennas Propagat.*, vol. AP-35, pp. 1418–1425, Dec. 1987.
[10] ——, "Electromagnetic scattering by a dielectric body with arbitrary inhomogeneity and anisotropy," *IEEE Trans. Antennas Propagat.*, vol. 37, pp. 384–389, Mar. 1989.
[11] S. C. Hill, C. H. Durney, and D. A. Christensen, "Numerical calculations of low-frequency TE fields in arbitrarily shaped inhomogeneous lossy dielectric cylinders," *Radio Sci.*, vol. 18, pp. 328–336, May 1983.
[12] D. H. Schaubert, D. R. Wilton, and A. W. Glisson, "A tetrahedral modeling method for electromagnetic scattering by arbitrarily shaped inhomogeneous dielectric bodies," *IEEE Trans. Antennas Propagat.*, vol. AP-32, pp. 77–85, Jan. 1984.
[13] C. T. Tsai, H. Massoudi, C. H. Durney, and M. F. Iskander, "A procedure for calculating fields inside arbitrarily shaped, inhomogeneous dielectric bodies using linear basis functions with the moment method," *IEEE Trans. Microwave Theory Tech.*, vol. MTT-34, pp. 1131–1138, Nov. 1986. (For comments, see *IEEE Trans. Microwave Theory Tech.*, vol. 35, pp. 785–786, Aug. 1987.).
[14] C. C. Su, "A procedure of solving the electric field integral equation for a dielectric scatterer with a large permittivity using face-centered node points," *IEEE Trans. Microwave Theory Tech.*, vol. 39, pp. 1043–1048, June 1991.
[15] M. R. Hestenes and E. Stiefel, "Method of conjugate gradients for solving linear systems," *J. Res. Nat. Bur. Stand.*, vol. 49, pp. 409–436, Dec. 1952.
[16] F. S. Beckman, "The solution of linear equations by the conjugate gradient method," in *Mathematical Methods for Digital Computers*, vol. 1, A. Ralston and H. S. Wilf, Eds. New York: Wiley, 1960, pp. 62–72.
[17] A. V. Oppenheim and R. W. Schafer, *Digital Signal Processing*. Englewood Cliffs, NJ: Prentice-Hall, 1976, p. 110.

Ching-Chuan Su was born in Taiwan, on October 2, 1955. He received the B.S., M.S., and Ph.D. degrees in electrical engineering from National Taiwan University in 1978, 1980, and 1985, respectively.

From 1980 to 1982, he was employed at the Industrial Technology Research Institute, Hsinchu, Taiwan, where he was responsible for the development of several IC fabrication processes for MOS products. In 1985 he joined the faculty of National Tsinghua University, Hsinchu, Taiwan, where he is an Associate Professor of Electrical Engineering. His research areas include fabrication of ferroelectric memory device, numerical solutions in scattering, waveguide, resonator, and MOS circuit, and electromagnetic theory.